

# Application of a GOY model to atmospheric boundary layer data

J. M. Vindel<sup>1</sup> and C. Yagüe<sup>2</sup>

<sup>1</sup>Área de Modelización, Agencia Estatal de Meteorología (AEMET), Madrid, Spain

<sup>2</sup>Dept. de Geofísica y Meteorología, Universidad Complutense de Madrid, Madrid, Spain

Received: 23 April 2009 – Revised: 11 August 2009 – Accepted: 8 September 2009 – Published: 12 October 2009

**Abstract.** This article analyzes the possibility of applying a GOY theoretical model to atmospheric boundary layer data. Bearing this in mind, relative scaling exponents of velocity structure functions are used to compare the model with the data under study. In the model, these exponents are set based on two parameters ( $q$  and  $\delta$ ), which are appropriate to define the model that better features a certain atmospheric state.

From these scaling exponents, the gap between 2-D and 3-D turbulence is observed in the model, depending on the fact that  $\delta$  is higher or lower than unity, respectively.

Atmospheric data corresponding to very different states of stratification stability have been analyzed. For convective or near-neutral situations (usually associated to 3-D turbulence), it is possible to find parameters  $q$  and  $\delta$  to define a model that fits the measured data. More stable situations can be featured by GOY models with higher values of  $\delta$ . However, it is clear that it is impossible to represent nocturnal situations of strong stable stratification (with a more similar behaviour to 2-D) with this type of model.

In the inertial range there is also a power relationship between any order structure function ( $S_p$ ) and order 3 structure function,  $S_3$  (ESS – Extended Self Similarity – method, Benzi et al., 1993). The exponents of this relationship,  $\overline{\zeta_p}$ , are called relative exponents, and its connection with  $\zeta_p$  is:

$$\overline{\zeta_p} = \zeta_p / \zeta_3 \quad (2)$$

There are several turbulence models (Frisch, 1995) which express the scaling exponent values according to one or several parameters. Shell models constitute an especially important group of models. These models consist of a set of equations obtained from the Navier-Stokes equations in Fourier space. For our study, from the many existing shell models, we select the GOY model, a more recent version of the Gledzer model (Gledzer, 1973) conceived by Yamada and Ohkitani (1987). An update information on shell models and in particular on GOY model can be found in Ditlevsen (2004).

This model uses a set of ordinary differential equations, each of them representative of a shell in which the Fourier space is divided, showing the following general form (the  $n$  sub-index refers to the  $n$ -th shell):

$$\left(\frac{d}{dt} + \nu k_n^2\right) u_n = i(a_n u_{n+1} u_{n+2} + b_n u_{n-1} u_{n+1} + c_n u_{n-1} u_{n-2})^* + f_n \quad (3)$$

where  $\nu$  represents kinematic viscosity,  $u_n$  velocity in the  $n$ -th shell ( $u_n=0$  for  $n \leq 0$ ),  $k_n$  the corresponding wave number (scale geometrically assumed, that is to say,  $k_n = k_0 q^n$ ) and  $f_n$ , a forcing term (if it is, for example, in the fourth mode,  $f_n = f \delta_{4,n}$ ).

With regard to the other coefficients,

$$a_n = a k_n = a k_0 q^n \quad b_n = b k_{n-1} = b k_0 q^{n-1} \quad c_n = c k_{n-2} = c k_0 q^{n-2} \quad (4)$$

So, the six parameters that define these models are:  $k_0$ ,  $q$ ,  $a$ ,  $b$ ,  $c$ , and  $f$ .

Usual values considered for some of those parameters (Kadanoff et al., 1995) are the following:

$$k_0 = 1/16; \quad a = 1; \quad q = 2; \quad f = 5(1+i)10^{-3} \quad (5)$$

## 1 Introduction

The velocity structure function of order  $p$ ,  $S_p$ , can be defined (for a temporal scale  $\tau$ ) as:

$$S_p(\tau) = \frac{\langle |u(t+\tau) - u(t)|^p \rangle}{\langle |u(t)|^p \rangle} \quad (1)$$

In the inertial range, there is a power relation between these structure functions and the scale, that is to say,  $S_p \propto \tau^{-\zeta_p}$ , where the coefficients  $\zeta_p$  are the so-called absolute scaling exponents.

According to Kolmogorov theory K41 (Kolmogorov, 1941), in conditions of homogeneity and isotropy, the scaling exponents,  $\zeta_p$ , have a linear dependence with regard to  $p$  order ( $\zeta_p = p/3$ ).



Correspondence to: J. M. Vindel  
(jmvindel@inm.es)

In the inviscid and the no-forcing case, the GOY model has two conserved integrals (Ditlevsen and Mogensen, 1996; Ditlevsen, 2004):

$$E = \frac{1}{2} \sum_n |u_n|^2 \quad \text{and} \quad E^2 = \frac{1}{2} \sum_n k_n^\alpha |u_n|^2 \quad \text{with} \quad q^\alpha = |\delta - 1|^{-1} \quad (6)$$

The first invariant corresponding to energy is valid for  $a+b+c=0$ . This condition we shall consider fulfilled from now on. In case of 3-D turbulence, according to the above mentioned Kolmogorov theory, energy describes a direct cascade with a  $-5/3$  slope. In the 2-D turbulence case (Kraichnan, 1967; 1971), energy describes an inverse cascade with that same slope, and enstrophy describes a direct cascade with a  $-3$  slope.

Assuming  $a$  to be the value given in Eq. (5),  $b$  and  $c$  could be expressed as a function of only one parameter,  $\delta$ :

$$b = -\delta; \quad c = \delta - 1 \quad (7)$$

Regarding the second invariant, if  $\delta < 1$ ,  $E^2$  is not positive and it can be written as:

$$E^2 = \frac{1}{2} \sum_n (-1)^n k_n^{Re(\alpha)} |u_n|^2 \quad (8)$$

In this case, when  $\alpha=1$ ,  $E^2$  can be identified with helicity, which is an inviscid invariant in the case of three-dimensional turbulence.

If  $\delta > 1$ ,  $E^2$  is always positive:

$$E^2 = \frac{1}{2} \sum_n k_n^\alpha |u_n|^2 \quad (9)$$

In this case, when  $\alpha=2$ ,  $E^2$  is identified with enstrophy which proves to be invariant in 2-D turbulence. Therefore, assuming 3-D turbulence, and assigning the value given in Eq. (5) to  $q$ ,  $\delta$  must be  $1/2$ , and, so:  $b=-1/2$  and  $c=-1/2$ . In the case of 2-D turbulence, and with the same  $q$  value,  $\delta$  must be  $5/4$ . In more general terms, when the parameter  $a$  is 1, if  $\delta$  exceeds 1, the turbulence is 2-D, as  $E^2$  is linked to enstrophy due to the fact that it is positive definite. On the contrary, if  $\delta$  is less than 1,  $E^2$  is non-positive definite, the same as the helicity, and the model refers to 3-D turbulence (Ditlevsen, 1996) (this critical point where the flux of energy changes sign and the helicity flux diverges, is also identified in Giuliani et al., 2002; see Constantin et al., 2007, for a generic  $a$ ).

On the other hand, the structure functions for each shell are calculated using the corresponding velocities:

$$S_p(n) = \langle |u_n|^p \rangle \quad (10)$$

satisfying the following scaling relation, which follows from the scaling properties of the governing equations:

$$S_p(n) \propto k_n^{-\xi_p} \quad (11)$$

## 2 Numerical simulations

For our numerical implementations, we shall carry out, like Pisarenko et al. (1993), a temporal discretization using a second-order slaved Adams-Bashforth scheme:

$$u_n(t+\delta t) = e^{-\nu k_n^2 \delta t} u_n(t) + \frac{1 - e^{-\nu k_n^2 \delta t}}{\nu k_n^2} \left( \frac{3}{2} g_n(t) - \frac{1}{2} g_n(t-\delta t) \right) \quad (12)$$

$g_n(t)$  being the right-hand side of Eq. (3).

To solve this equation and ensure stability of integration and consistent outcomes, the following conditions will be considered: for the study of atmospheric turbulence, we shall use a characteristic value of viscosity in this environment:  $\nu = 1.8 \times 10^{-5} \text{ m}^2 \text{ s}^{-1}$ ; the total number of time steps will be  $4 \times 10^4$ , and  $\delta t$  time step will be  $10^{-4}$  or  $10^{-3}$ , for a better statistical significance in the results. Also, the number of shells to be considered is  $N=22$ .

For our first simulation, a standard situation in 3-D will be considered: the values indicated in Eq. (5) and  $\delta=1/2$ . To deal with this case, we have used a time step of  $10^{-3}$ .

In Fig. 1, structure functions in logarithmic scale versus shell index have been represented. The slopes of these graphs therefore correspond with the scaling exponents. A maximum is observed towards shell number 4 (where forcing has been introduced); and, around shell number 15, a noticeable change occurs in the slopes of all graphs.

Applying the ESS condition, we have represented  $\log(S_p)$  vs.  $\log(S_3)$  to determine the relative scaling exponents (Fig. 2). Least square linear matching proves to be much more accurate to calculate slopes than in Fig. 1 and, in addition, there is no need to restrict shell numbers to carry it out. For that reason, we will implement this procedure instead of using Eq. (11), and later we shall estimate the dependency of the relative exponents with the characteristic parameter values of a GOY model (the ESS method is also used to study the intermittency in Paret and Tabeling (1998), as this condition provides a better defined and larger scaling range than the curve  $S_p$  vs. scale).

We are interested in dealing with the relative scaling exponents reflected by the model when  $q$  and  $\delta$  values are modified (Bowman et al., 2006). The rest of the parameters will remain constant and the above mentioned values will be considered.  $\delta$  (with 0.05 intervals) varies in the range [0.2–1.8] (except for  $\delta=1$ ) and  $q$  (with 0.1 intervals) between [1.6–2.3]. Within those ranges, maintaining the above mentioned working conditions (but using a  $10^{-4}$  time step), the results have the necessary stability. In order to limit the uncertainty in the determination of scaling exponents, we have only calculated up to order 5. The lines of fit to the curves  $S_p$  vs.  $S_3$  (in log-log) show, in all cases, a determination coefficient higher than 0.99 (except for the case of  $q=1.6$  and  $\delta=0.2$ , where  $R^2=0.9873$  is obtained). We should point out that the matching has been made using, in all cases, only the first 11 shells, as there are situations in which, in higher shells,

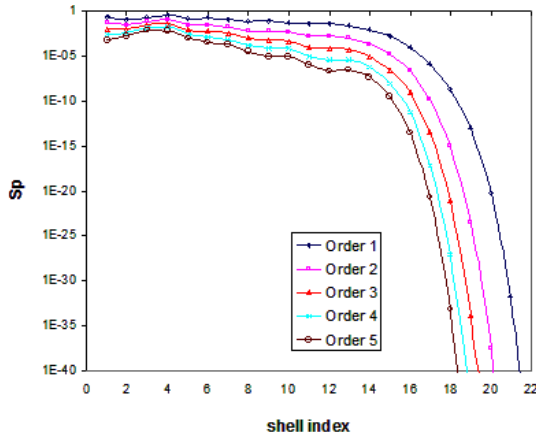


**Fig. 1.** Structure functions (logarithmic scale) vs. shell index.

structure functions are declared null, making the estimation of their logarithms impossible.

In Fig. 3 we have represented the relative scaling exponents as a function of the parameter  $\delta$  (for different values of the parameter  $q$ ). In this figure, a gap between 2-D and 3-D turbulence is observed, depending on the fact that  $\delta$  is higher or lower than unity, respectively. This critical point coincides, as we pointed out in the introduction, with the value for which the second inviscid invariant is positive or not. In the three-dimensional region, the scaling exponents diminish (for  $p < 3$ ) or increase (for  $p > 3$ ) when we approach the 2-D area. In the 3-D area, it is even possible to establish a functional relationship between the scaling exponents and the  $\delta$  parameter with a high correlation coefficient. For instance, for  $q=1.8$ , we obtain:

$$\begin{aligned} \bar{\zeta}_1 &= 0.9586\delta^4 - 2.8408\delta^3 + 3.2006\delta^2 - 1.7048\delta + 0.7298 \\ \bar{\zeta}_2 &= 0.56\delta^4 - 1.6593\delta^3 + 1.8686\delta^2 - 0.9935\delta + 0.8968 \\ \bar{\zeta}_4 &= -0.623\delta^4 + 1.8471\delta^3 - 2.0809\delta^2 + 1.1054\delta + 1.078 \\ \bar{\zeta}_5 &= -1.2776\delta^4 + 3.7892\delta^3 - 4.2701\delta^2 + 2.2684\delta + 1.143 \end{aligned} \quad (13)$$

with a very high determination coefficient: 0.9999.

Nevertheless, in the 2-D region the scaling exponents depict a figure quite constant and linear.

The shape of the graphs in Fig. 3 confirms the foreseeable diminution of the intermittency in 2-D turbulence (Smith and Yaghot, 1993; Paret and Tabeling, 1998). Indeed, due to Hölder inequality (Frisch, 1995), the relationship  $\zeta_p$  vs.  $p$  presents a concave shape. That is to say, for  $p$  less than order 3, the smaller the scaling exponent, the higher the proximity of the graph to the linear form and the smaller will thus be the intermittency (in Fig. 3a and b, when approaching the 2-D turbulence, the scaling exponents decrease, the same as intermittency). On the other hand, for orders higher than 3, a smaller intermittency must imply higher values of the scaling exponents (that is to say, when approaching the 2-D, the scaling exponents increase – Fig. 3c and d). The reason for

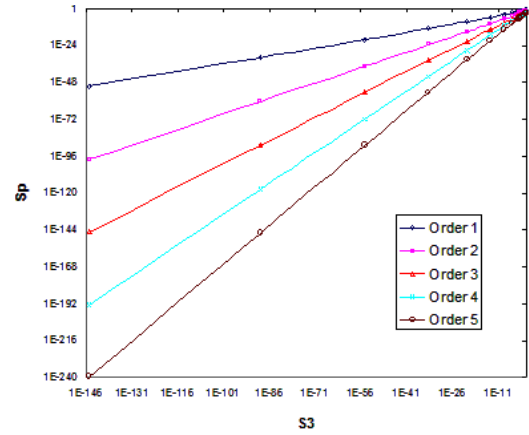


**Fig. 2.** Different orders structure functions (logarithmic scale) vs. order 3 structure function (logarithmic scale).

the weak intermittency in 2-D could be due to the lack of intense vortex filaments (responsible for intermittent bursts) in 2-D turbulence (Daniel and Rutgers, 2000).

Similarly, the  $\delta$  parameter being fixed, we can represent the variation of the scaling exponents with the  $q$  parameter. This is shown in Fig. 4. In this case, for  $\delta < 1$  it is also possible to establish a functional relationship between the relative scaling exponents and  $q$  with a high correlation coefficient; for example, for  $\delta=0.5$ , we have (with a determination coefficient of 0.9996):

$$\begin{aligned} \bar{\zeta}_1 &= 0.0657q^4 - 0.729q^3 + 2.8711q^2 - 4.8708q + 3.4109 \\ \bar{\zeta}_2 &= 0.0759q^4 - 0.7358q^3 + 2.6367q^2 - 4.1659q + 3.1454 \\ \bar{\zeta}_4 &= -0.1136q^4 + 1.0586q^3 - 3.6741q^2 + 5.65q - 1.9455 \\ \bar{\zeta}_5 &= -0.2487q^4 + 2.3005q^3 - 7.9325q^2 + 12.13q - 5.3347 \end{aligned} \quad (14)$$

In order to have a measurement of the uncertainty existing in the previous figures, in Fig. 5 we have represented some cases with the error bars (with a confidence interval of 99%). Figure 5a shows that uncertainty increases when  $\delta$  decreases (from  $\delta=0.8$  approximately). On the other hand, the parameter  $q$  (Fig. 5b) does not affect very much the degree of uncertainty on scaling exponents. However, the more distant the orders are from  $p=3$ , the greater the uncertainty presented in the relative scaling exponents.

### 3 Data and empirical results

In the previous section, we analyzed the relative scaling exponents, relating them to the typical parameters of the GOY model. Next, we shall study the possibility of applying the previously defined structure to real atmospheric boundary layer data, through the relative scaling exponents.

A study of anomalous scaling has been done instead to study just the scaling, although the latter can be more robust

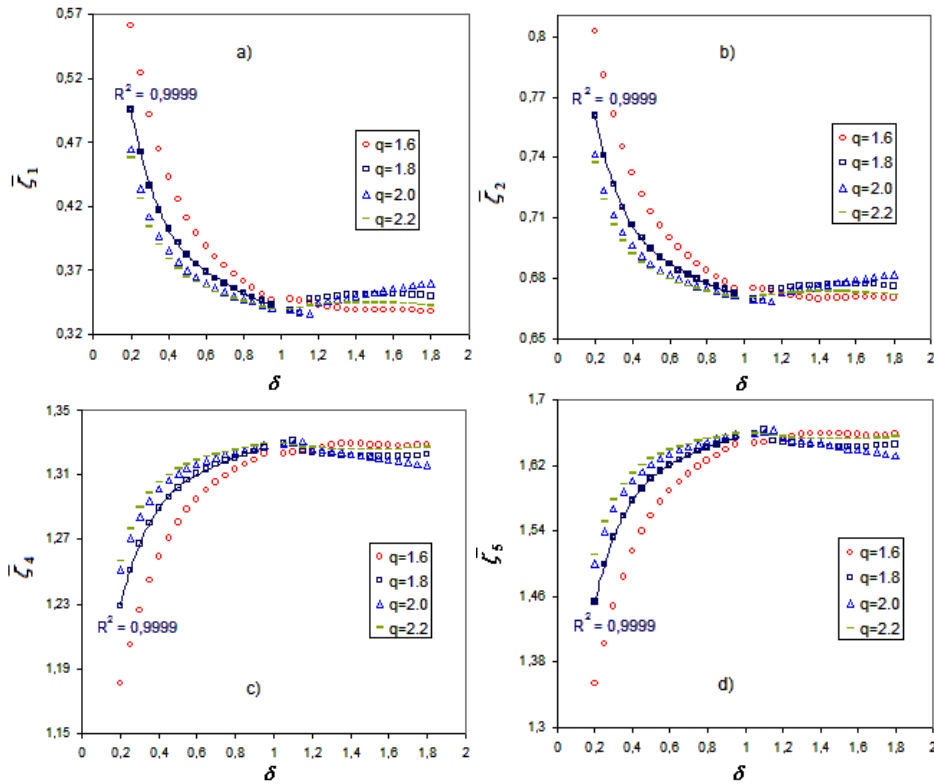


**Fig. 3.** Relative scaling exponents for different values of the  $q$  parameter vs.  $\delta$  for: (a) order 1, (b) order 2, (c) order 4 and (d) order 5. A solid line represents a 4-th order polynomial fit for  $q=1.8$  after Eq. (13) (determination coefficient is shown).

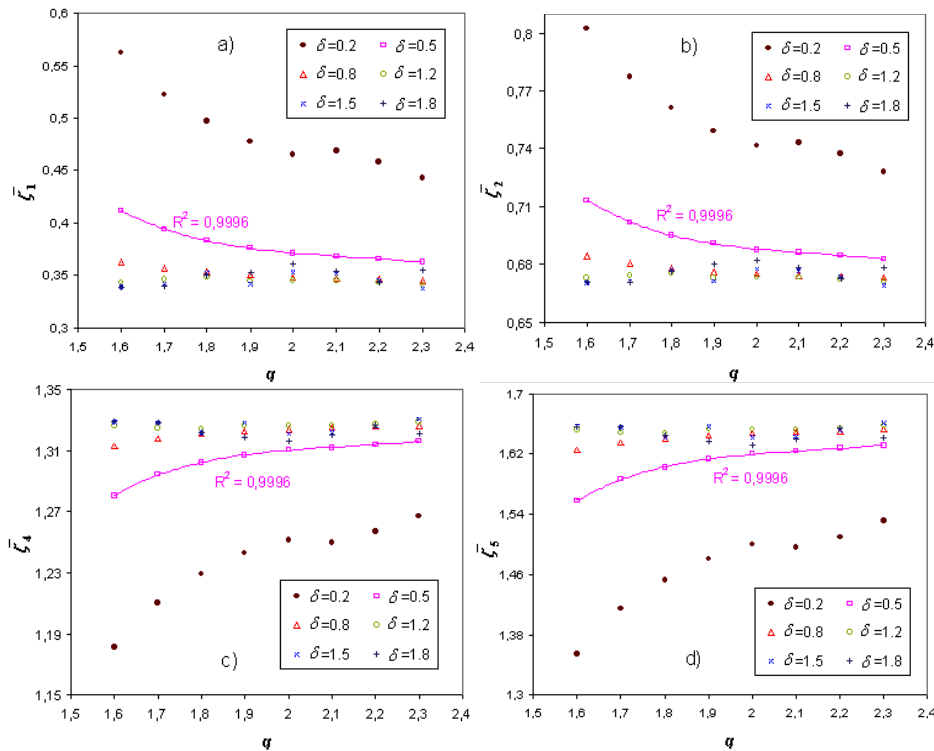


**Fig. 4.** Relative scaling exponents for different values of the  $\delta$  parameter vs.  $q$  for: (a) order 1, (b) order 2, (c) order 4 and (d) order 5. A solid line represents a 4-th order polynomial fit for  $\delta=0.5$  after Eq. (14) (determination coefficient is shown).

to determine differences between 2-D and 3-D turbulence. However, the study of just the scaling is different in both types of turbulence, and this should be known a priori for each study situation. Although we can assume that nights are in general more stable and thus, more similar to 2-D turbulence (neither in the nature nor in the laboratory turbulence can be 2-D in a strict sense), we cannot use a specific value of  $\Delta T_{50-0.22}$  to separate the character of the atmospheric turbulence (2-D or 3-D).

Data from a sonic anemometer (20 Hz sampling rate) at 32 m have been used. This data was collected during the SABLES98 (Stable Atmospheric Boundary Layer Experiment in Spain) field campaign, which took place in September 1998 at the Research Centre for the Lower Atmosphere (CIBA, 41°49' N, 4°56' W, 840 m a.g.l.), located at a flat and homogeneous terrain in the centre of an extensive plateau (Montes Torozos). The site is surrounded by fairly level grass plains, with a surface roughness  $z_0=10^{-4}$  m (San José et al., 1985). The Duero river flows along the SE border of the plateau and two small river valleys, which may act as drainage channels in stable conditions, extend from the lower SW region of the plateau. The main instrumentation (3 sonic anemometers, 5 cup anemometers, 14 thermocouples, 3 wind vanes, a fast humidity sensor, an infrared surface temperature sensor, a radiometer and a barometer) was installed on the 100 m meteorological tower. This instrumentation was provided (and calibrated) by the Risø National Laboratory. The sonic anemometers levels were 5.8 m, 13.5 m and 32 m. The sampling rate for the sonic anemometers was set up to 20 Hz, while the thermocouples, wind vanes and cup anemometers were sampling at 5 Hz. Five-minutes means were used for evaluating mean and stability parameters. Prior to the calculation of these means, the raw data from the sonic anemometers was pre-processed to align the sonic axes along the five-minutes mean flow direction. For further details on the rotation of the sonic axes, Kaimal and Finnigan (1994) can be consulted. An extensive report on the instrumentation used and the characteristics of SABLES98 can be found in Cuxart et al. (2000).

The period of study will be between 10 September at 17:00 GMT and 17 September at 23:30 GMT, with information taken at intervals of 30 min (in total, 350 samples to be studied). These data correspond to very different stability situations from diurnal convection to very strong stable nights and therefore cover a wide scale of turbulent situations. For each of these samples we shall use intervals of 5 min (6000 items of data), which is an optimal compromise between using enough data to provide statistics and avoiding mesoscale motion influences, since we are interested in the turbulent scales (Stull, 1988).

In Fig. 6, we have represented the difference of temperatures between 50 m and 0.22 m levels,  $\Delta T_{50-0.22}$ , so as to show the evolution of stability of stratification throughout the period of study (to make the daytime cycle, which shows stratification stability, more visible, we have modulated the

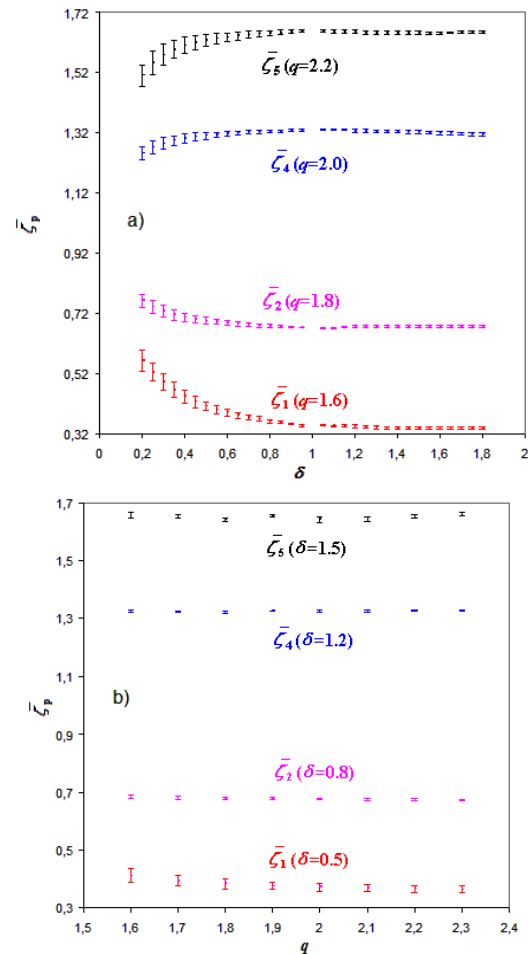


**Fig. 5.** (a) Relative scaling exponents vs.  $\delta$  (for different values of  $q$ ) with error bars; (b) Relative scaling exponents vs.  $q$  (for different values of  $\delta$ ) with error bars.

curve using a moving average of order 12, that is to say, of 6 h). The graph shows the typical increase of stability during the night, with large and positive values of  $\Delta T_{50-0.22}$  which in this case represents the strength of the surface-based inversion developed during clear skies and low wind nights. On the other hand during strong surface heating, taking place along the diurnal times,  $\Delta T_{50-0.22}$  has large and negative values, being more negative as the convection is more important. We have also estimated the relative scaling exponents (orders 1, 2, 4 and 5) corresponding to the different situations of study (in Fig. 6, 2nd and 5th orders have been represented). A scaling range of 30 s/20 (1/20 s is the sonic anemometer resolution) has been used to obtain the scaling exponents and, in almost all of the cases, the determination coefficient of the  $S_p$  vs.  $S_3$  fit, from a power relationship, is higher than 0.99 (the lowest  $R^2$  are: 0.9374 for  $\zeta_1$ , 0.982 for  $\zeta_2$ , 0.9744 for  $\zeta_4$ , and 0.8867 for  $\zeta_5$ ). We have chosen the length of the scaling range (up to 30) in order to have a minimum number of points for the fit and to fulfil the ESS condition. The range extends along the smallest scales, covering the dissipation

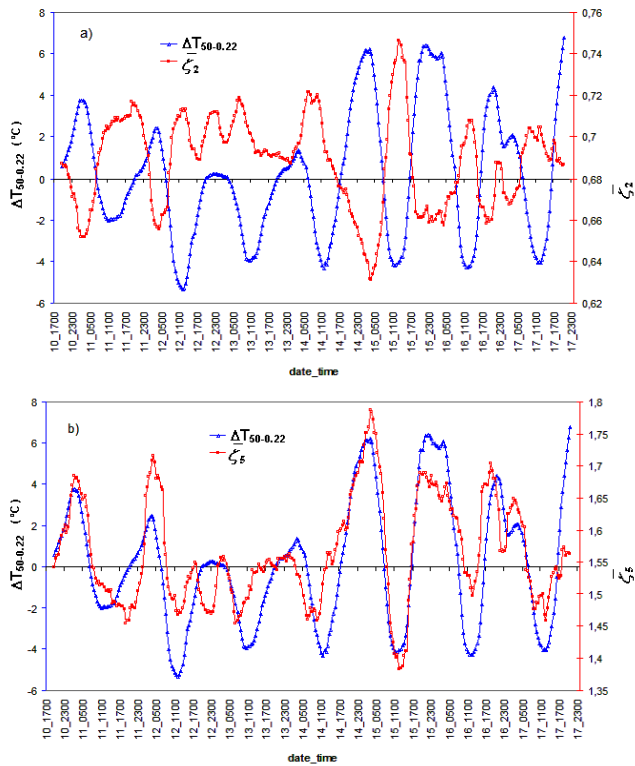


**Fig. 6.** Temporal evolution of temperature difference between 50 m and 0.22 m levels,  $\Delta T_{50-0.22}$ , (left axis) and relative scaling exponents (right axis) for: (a) order 2,  $\zeta_2$ , (b) order 5,  $\zeta_5$ .

range and the last part of the inertial range (some characteristic scales as the Kolmogorov and integral scales can be seen in Vindel et al., 2008). A moving average of order 12 has also been used for the scaling exponents, similarly to the temperature difference between 50 m and 0.22 m. There is a clear relationship between the values of the scaling exponents and the corresponding situation of stability and it is shown a different behaviour for  $\zeta_2 (p < 3)$  compared to  $\zeta_5 (p > 3)$ . The reason could be due to the relation between the atmospheric stability and the kind of turbulence: convective to near-neutral situations, usually associated to 3-D turbulence, and stable situations (often 2-D). In the above Sect. 3, a further explanation can be found about the relationship shown in Fig. 3 between scaling exponents and 2-D and 3-D turbulence.

In order to show the possible application of the GOY model to atmospheric data, the relative scaling exponents corresponding to the studied situations have been plotted in Fig. 7. In this figure, we have also included the maximum and minimum values of the scaling exponents for certain values of parameter  $q$  of the model. Figure 3 showed that, for orders lower than 3, situations closer to 2-D turbulence (as in cases of stronger stability) have lower scaling exponents than situations more embedded in the 3-D area (as is the case with more unstable situations) and that, for orders higher than 3, the behaviour of the scaling exponents is the

opposite. Figure 7 also exhibits a similar behaviour. Indeed, the shape of the graphs of orders lower than 3 corresponding to the different situations of study (with minimum values in more stable situations), is similar to that of the graphs of orders higher than 3 (but reversed, as shown in the shape of the graphs of Fig. 3). This Fig. 7 shows that there are certain atmospheric situations (coinciding with those more stably-stratified) in which the model is unable to represent their corresponding scaling exponents (for example those situations present in the 14–15 night, where very strong stable stratification was observed – Yagüe et al., 2006 –), due to the fact that the scaling exponents are too high (for orders higher than 3) or too low (for orders lower than 3) for the model. Moreover, the minimum values (for orders lower than 3) or maximum values (for orders higher than 3) of the scaling exponents that the model is able to reproduce are very similar for different  $q$  values (see Fig. 3).

Figure 8 is similar to Fig. 7, apart from the fact that the maximum and minimum values of the scaling exponents have been obtained for certain values of parameter  $\delta$ . It is interesting to observe that, as the value of  $\delta$  increases, the model is capable of representing more stable situations. However, we again observe that the model is unable to show the exponents corresponding to atmospheric situations of greater stability.

If we wish to obtain the values of the parameters of the model that provide scaling exponents comparable to those of a given atmospheric situation, we have to use the relations (13), (14) and similar. Nevertheless, it should be borne in mind that each model furnished by a pair of parameters  $q$  and  $\delta$ , can only represent the scaling exponents of a certain order.

#### 4 Summary and conclusions

A simulation of a GOY model of 22 shells (using standard atmospheric viscosity), was performed to calculate the scaling exponents of the structure functions from the ESS method, which proves to be more accurate than the direct use of the power scaling relationship.

Different simulations using different values of the characteristic parameters of a GOY model were then carried out. As a result, two areas with different behaviour corresponding to 2-D and 3-D turbulence can be clearly distinguished. The values of the scaling exponents in one region and in the other confirm the behaviour of the intermittency in one type of turbulence and in the other (a decrease of the scaling exponents of order lower than 3 when we move to 2-D from 3-D, and the reverse behaviour for cases of order higher than 3).

Replacing the relative scaling exponents corresponding to a certain atmospheric situation with the expressions (13), (14) and similar, it is possible to estimate a pair of parameters  $q$ ,  $\delta$ , that will define the appropriate model to represent the



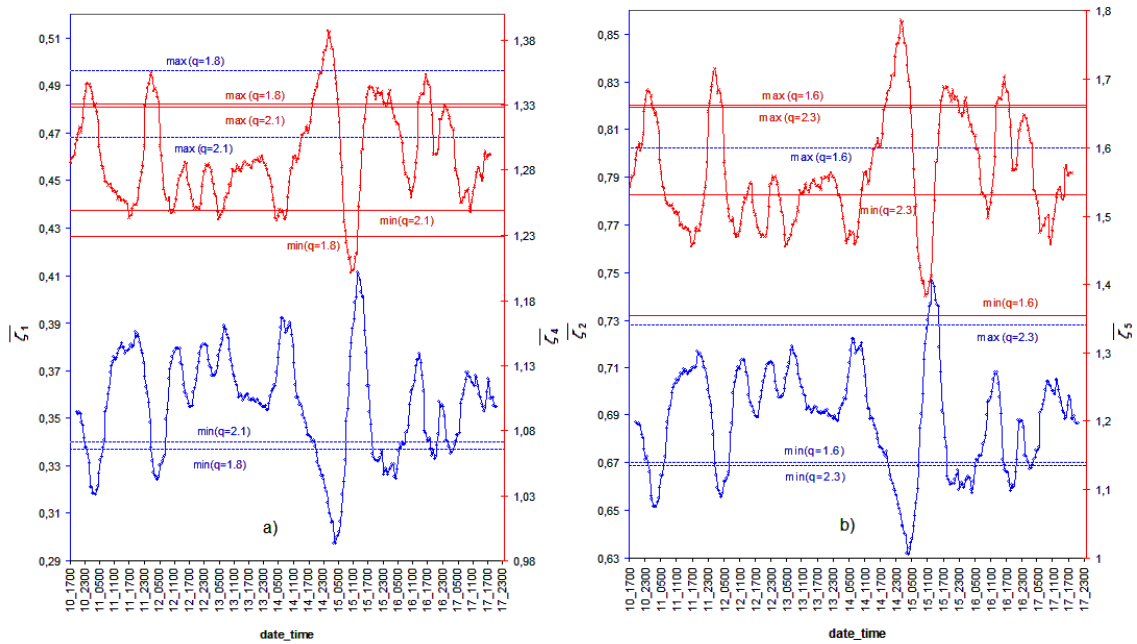


**Fig. 7.** (a) Temporal evolution of relative scaling exponents of order 1 (left axis) and order 4 (right axis). The horizontal lines represent the maximum and minimum values of  $\bar{\zeta}_1$  (dashed lines) and  $\bar{\zeta}_4$  (solid lines) for certain values of parameter  $q$  of the model; (b) Similar to (a) for orders 2 and 5.

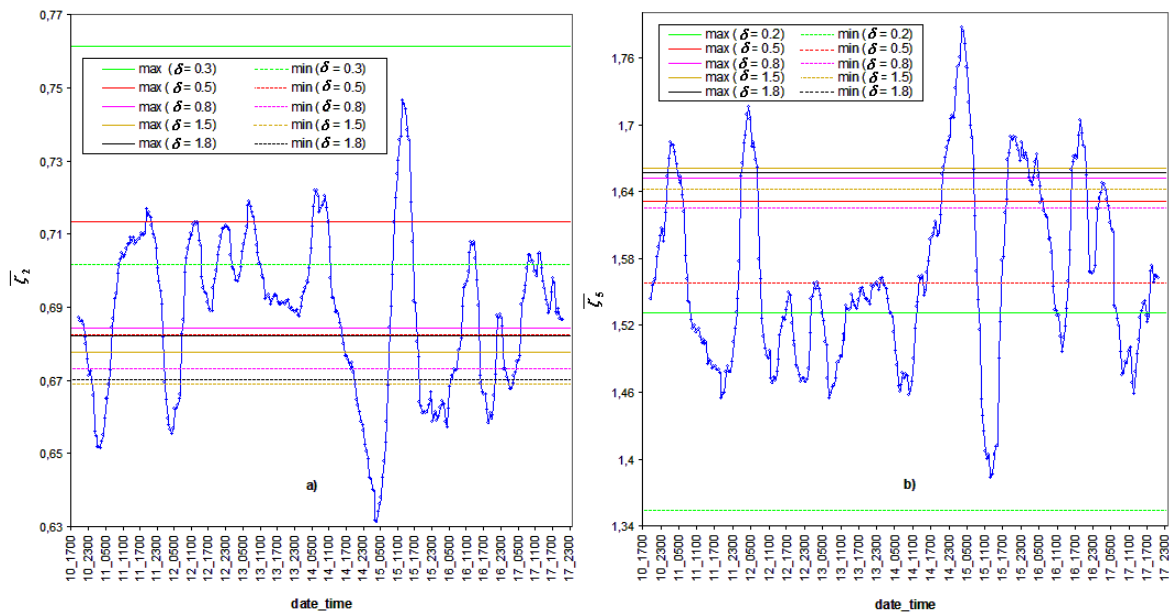


**Fig. 8.** (a) Temporal evolution of relative scaling exponents of order 2. The horizontal lines represent the maximum (solid) and minimum (dashed) values of  $\bar{\zeta}_2$  for certain values of parameter  $\delta$  of the model; (b) Similar to (a) for order 5. Note that the black dashed line overlapped the red solid line.

scaling exponent of a certain order for that situation. Overall, all of them enable the representation of the given atmospheric situation. Greater values of the parameter  $\delta$  produce a model which is able to represent increasingly stable situations. But the model is of no use in situations of stronger stability of stratification.

*Acknowledgements.* This research has been funded by the Spanish Ministry of Science and Innovation (projects CGL 2006-12474-C03-03 and CGL2009-12797-C03-03). GR58/08 program (supported by BSCH and UCM) has also partially financed this work through the Research Group “Micrometeorology and Climate Variability” (no 910437). Thanks are also due to the referees who have deeply improved the initial manuscript.

Edited by: A. Provenzale

Reviewed by: A. M. Tarquis and another anonymous referee

## References

- Benzi, R., Ciliberto, S., Tripicciono, R., Baudet, C., Massaioli, F., and Succi, S.: Extended self-similarity in turbulent flows, *Phys. Rev. E*, 48, 29–36, 1993.
- Bowman, J. C., Doering, C. R., Eckhardt, B., Davoudi, J., Roberts, M., and Schumacher, J.: Links between dissipation, intermittency and helicity in the GOY model revisited, *Physica D*, 218, 1–10, 2006.
- Constantin, P., Levant, B., and Titi, E. S.: A note on the regularity of inviscid shell models of turbulence, *Phys. Rev. E*, 75(1), 016304, 1–10, 2007.
- Cuxart, J., Yagüe, C., Morales, G., Terradellas, E., Orbe, J., Calvo, J., Fernández, A., Soler, M. R., Infante, C., Buenestado, P., Espinalt, A., Joergensen, H. E., Rees, J. M., Vila, J., Redondo, J. M., Cantalapiedra, I. R., and Conangla, L.: Stable Atmospheric Boundary-Layer Experiment in Spain (SABLES 98): A Report, *Bound.-Lay. Meteorol.*, 96(3), 337–370, 2000.
- Daniel, W. B. and Rutgers, M. A.: Intermittency in forced two-dimensional turbulence, *arXiv:nlin/0005008v1 [nlin.CD]*, 3 May 2000.
- Ditlevsen, P. D.: Temporal intermittency and cascades in shell models of turbulence, *Phys. Rev. E*, 54(1), 985–988, 1996.
- Ditlevsen, P. D. and Mogensen, I. A.: Cascades and statistical equilibrium in shell models of turbulence, *Phys. Rev. E*, 53(5), 4785–4793, 1996.
- Ditlevsen, P. D.: Turbulence and climate dynamics, *Print J&R Frydenberg A/S, Copenhagen*, 349 pp., 2004.
- Frisch, U.: *Turbulence*, England: Cambridge University Press, 296 pp., 1995.
- Giuliani, P., Jensen, M. H., and Yakhot, V.: Critical “dimension” in shell model turbulence, *Phys. Rev. E*, 65(3), 036305, doi:10.1103/PhysRevE.65.036305, 2002.
- Gledzer, E. B.: System of hydrodynamic type admitting two quadratic integrals of motion, *Soviet Physics Doklady*, 18, 216–217, 1973.
- Kadanoff, L., Lohse, D., Wang, J., and Benzi, R.: Scaling and dissipation in the GOY shell model, *Phys. Fluids*, 7(3), 617–629, 1995.
- Kaimal, J. C. and Finnigan, J. J.: *Atmospheric Boundary Layer Flows: Their Structure and Measurements*, Oxford University Press, New York, 289 pp., 1994.
- Kolmogorov, A. N.: Dissipation of energy in locally isotropic turbulence, *C. R. Acad. Sci. USSR*, 32, 16–18, 1941.
- Kraichnan, R. H.: Inertial ranges in two-dimensional turbulence, *Phys. Fluids*, 10(7), 1417–1423, 1967.
- Kraichnan, R. H.: Inertial-range transfer in two- and three-dimensional turbulence, *J. Fluid Mech.*, 47(3), 525–535, 1971.
- Paret, J. and Tabeling, P.: Intermittency in the two-dimensional inverse cascade of energy: experimental observations, *Phys. Fluids*, 10, 3126–3136, 1998.
- Pisarenko, D., Biferale, L., Courvoisier, D., Frisch, U., and Vergasola, M.: Further results on multifractality in shell models, *Phys. Fluids A-Fluid*, 5(10), 2533–2538, 1993.
- San Jose, R., Casanova, J. L., Viloria, R. E., and Casanova, J.: Evaluation of the Turbulent Parameters of the Unstable Surface Boundary Layer outside Businger’s Range, *Atmos. Environ.*, 19, 1555–1461, 1985.
- Smith, L. M. and Yakhot, V.: Condensation and small-scale structure generation in a random force driven 2D turbulence, *Phys. Rev. Lett.*, 71, 352–355, 1993.
- Stull, R. B.: *An Introduction to Boundary Layer Meteorology*, Atmospheric Sciences Library, Kluwer Academic Publishers, 666 pp., 1988.
- Vindel, J. M., Yagüe, C., and Redondo, J. M.: Structure function analysis and intermittency in the atmospheric boundary layer, *Nonlin. Processes Geophys.*, 15, 915–929, 2008, <http://www.nonlin-processes-geophys.net/15/915/2008/>.
- Yagüe, C., Viana, S., Maqueda, G., and Redondo, J. M.: Influence of stability on the flux-profile relationships for wind speed,  $\phi_m$ , and temperature,  $\phi_h$ , for the stable atmospheric boundary layer, *Nonlin. Processes Geophys.*, 13, 185–203, 2006, <http://www.nonlin-processes-geophys.net/13/185/2006/>.
- Yamada, M. and Ohkitani, K.: Lyapunov spectrum of a chaotic model of three-dimensional turbulence, *J. Phys. Soc. Jpn.*, 56, 4210–4213, 1987.